**NATIONAL TECHNICAL UNIVERSITY OF UKRAINE**
**“IGOR SIKORSKY KYIV POLYTECHNIC INSTITUTE”**
FACULTY OF BIOMEDICAL ENGINEERING
DEPARTMENT OF BIOMEDICAL ENGINEERING

«Admission to the defense»
Head of the Department of BMI
________ Vladyslav SHLYKOV
(signature)
“ ______ ” _____________2023

**Diploma thesis**

**to obtain a bachelor's degree**

**on the educational and professional program** «Medical engineering»

**in the specialty** 163 «Biomedical engineering»

**on the subject: «Processing of thermographic images of brain vessels»**

Completed:
4th year student, group BM-93i,
Mahmoud Hassan Sabha
(Full Name) (signature)

Head:
Assoc. Prof., Doctor of Engineering,
Vladyslav Shlykov
(Full Name) (signature)

Consultant from section SAFETY AND LABOR PROTECTION:
Assoc. Prof. of the department of power supply, PhD,
Vasyl Kalinchyk
(Full Name) (signature)

Reviewer:
Assistant of the Department of Biosafety and Human Health,
Intellectual Danylo
(Full Name) (signature)

I certify that in this master's dissertation there are no borrowings from the works of other authors without appropriate references.

Student ___________________
(signature)

KYIV - 2023

**NATIONAL TECHNICAL UNIVERSITY OF UKRAINE**
**“IGOR SIKORSKY KYIV POLYTECHNIC INSTITUTE”**
FACULTY OF BIOMEDICAL ENGINEERING
DEPARTMENT OF BIOMEDICAL ENGINEERING

Level of education Diploma
Specialty 163 «Biomedical engineering»
(code and name)

I APPROVE
Head of the Department of BMI
________ Vladyslav SHLYKOV
(signature)
“ ______ ” ______________2023

# TASK

## for a student's diploma thesis

Mahmoud Hassan Sabha
(Full Name)

1. topic Processing of thermographic images of brain vessels

scientific supervisor of the dissertation Vladyslav SHLYKOV, Doctor of Engineering, Associate Professor
(last name, first name, patronymic, academic degree, academic title)

approved by the order of the university № 52/23-si from 05/26/2023

2. The deadline for students to submit a dissertation 14.06.2023

3. The object of study is Brain blood vessels

4.The subject of the research is

Processing of thermographic images of brain vessels

5. List of tasks to be developed to create software that can detect pathologies of brain blood vessels (arteries, veins, lymphatic channels) based on the temperature profile distribution, and the use of thermographic images of brain vessels obtained through the Flir i7 thermal imager to develop a software product for processing and analyzing these images.

6. Approximate list of graphic material 23 tables, 27 figures

7. Approximate list of publications:

Create software that can detect pathologies of brain blood vessels based on the temperature profile distribution.

8. Date of issue of the task 05.04.2023

Calendar plan

| № з/п | Name of stages of execution diploma thesis | Deadline for stages diploma thesis | Note |
|---|---|---|---|
| 1 | Analysis of scientific literature and patent databases on a given topic | 20.04.2023 | |
| 2 | Development of the content and structure of MD | 28.04.2023 | |
| 3 | Investigation of structures of oncological neoplasms in the heart | 08.05.2023 | |
| 4 | Development of a method of contouring oncological formations on MRI images of the heart | 15.05.2023 | |
| 5 | Experimental testing of the method of contouring volumetric formations in the heart on the existing clinical basis of MRI images of the heart | 26.05.2023 | |
| 6 | Registration of MD | 31.05.2023 | |
| 7 | Getting a review and feedback | 01.06.2023 | |
| 8 | Passing norm control | 09.06.2023 | |
| 9 | MD protection | 14.06.2023 | |

Student ____________ Mahmoud Sabha
(signature) (initials, surname)

Supervisor of the dissertation ____________ Vladyslav Shlykov
(signature) (initials, surname)

# ABSTRACT

The present thesis is a 76-page document comprising 3 chapters, 19 illustrations, 15 tables, 3 appendices, and a list of references with 5 sources. The focus of the study is the use of thermographic images of brain vessels obtained through the Flir i7 thermal imager to develop a software product for processing and analysing these images. The aim of the work is to create software that can detect pathologies of brain blood vessels (arteries, veins, lymphatic channels) based on the temperature profile distribution.

The first chapter provides an overview of the history, theory, and application of infrared radiation. The second chapter discusses theoretical and practical methods of thermal image analysis, while the third chapter focuses on labour protection.

The results of this research can be applied to the analysis of thermal images of the human brain, allowing for the identification of blood vessel pathologies such as stenosis or occlusion.

Table of Contents

# Introduction

Today, an actual problem in medicine is the analysis of the arteries of the human brain to detect the pathology of blood vessels (arteries, veins, lymphatic channels), atherosclerotic changes in the vessels.

Thermal imaging is used in the diagnosis of heart diseases, assessment of kidney function and the detection of cysts and tumours in them, detection of aneurysms - pathological expansions of blood vessels, tumours, blood clots, arteriovenous shunts (pathological junctions of arteries and veins) in the brain, as well as for the diagnosis of retinal diseases.

The world practice in medicine shows that a complex analysis of a patient, using all possible methods, gives more accurate results than individual analyses, which affects the number of deaths of people.

The purpose of this work is to analyse the method of thermographic digital imaging of the arteries of the human brain to further determine the reliability of this method.

The main goal of this work is to analyse the method for detecting the arteries of the human brain using thermal imaging. By studying the properties of the image captured on thermal images it is possible to develop algorithms that can be used for digital analysis of the arteries in the brain. For this study, it is proposed to use the method of image processing to identify arteries in the human brain.

The method of image processing consists of three steps: pre-processing of the image; segmentation of the image based on pixel values; and classification based on the patterns found in the segmented region. Pre-processing is done to remove noise from an image such as blurring or compression artifacts.

Segmentation is performed to separate objects of interest from the background. Classification is applied to assign each object into one or more classes by calculating the respective probabilities of belonging to each class. The ultimate goal is to find an accurate and fast algorithm for recognizing arteries in thermal images of the brain. This will help the physician in making accurate diagnosis for patient care.

# 1. GENERAL PART

## 1.1 Historical information

The study of infrared radiation has a long history dating back to the late 18th century, when Swedish chemist Karl Scheele described the properties and production of "fiery air" in his work "Chemical Treatise on Air and Fire". In 1777, Lambert experimentally demonstrated that heat rays travel in a straight line and their intensity decreases inversely proportional to the square of the distance. In the early 1800s, William Herschel began measuring temperature outside the spectrum and discovered the presence of invisible rays with the greatest heating power. By 1830, Herschel's experiments had been repeated enough times to confirm the existence of these invisible rays, which were outside the red part of the visible solar spectrum and caused the mercury bulb of a thermometer to heat up. These rays were later called infrared by French physicist Becquerel. In 1893, German physicist Wilhelm Wien determined that the wavelength corresponding to the maximum radiation energy of an absolutely black body is inversely proportional to the absolute temperature. In 1934, the development of an electron-optical converter allowed for the transformation of invisible infrared, ultraviolet, and X-ray images of an object into visible ones.

## 1.2 Theoretical information

Infrared radiation is a type of electromagnetic radiation with a wavelength that is longer than that of visible light, typically ranging from 750 nm to 1 mm (Fig. 1.2.1). While the human eye is unable to detect infrared radiation, some animals, such as snakes and bats, have sensory organs that can sense this type of radiation and use it to navigate in low light conditions.

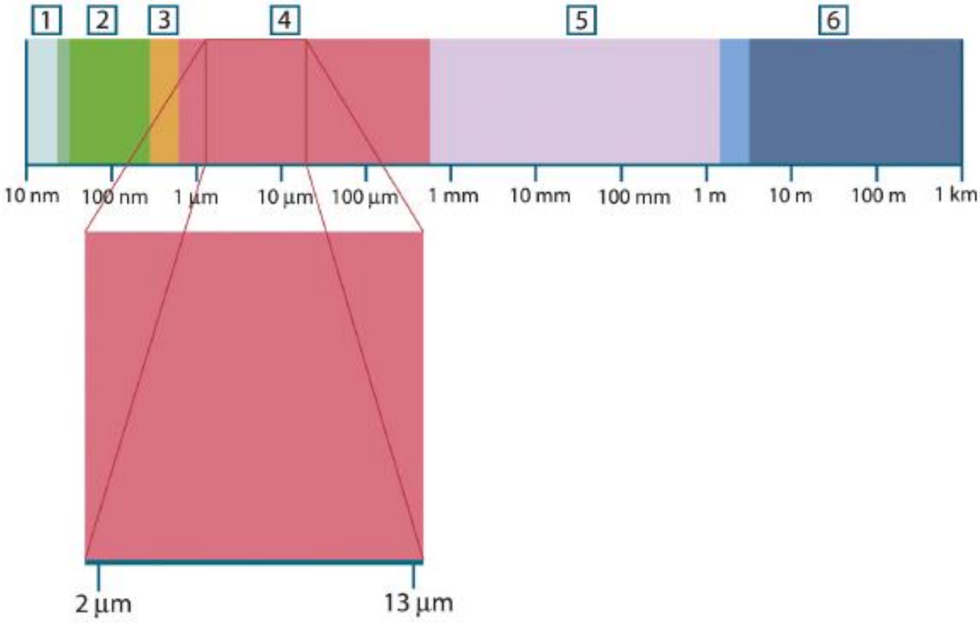


Figure 1.2.1 – Electromagnetic spectrum: 1: X-ray waves; 2: ultraviolet waves; 3: visible range; 4: infrared radiation; 5: microwaves; 6: radio waves;

Infrared radiation is emitted by all objects with a temperature higher than absolute zero. The intensity of this radiation depends on the temperature of the object. As the temperature increases, the maximum intensity of the radiation shifts towards shorter wavelengths, which can eventually be within the range of visible light. Due to the relationship between the spectrum and intensity of infrared radiation and temperature, it is often referred to as thermal radiation (Fig. 1.2.2).

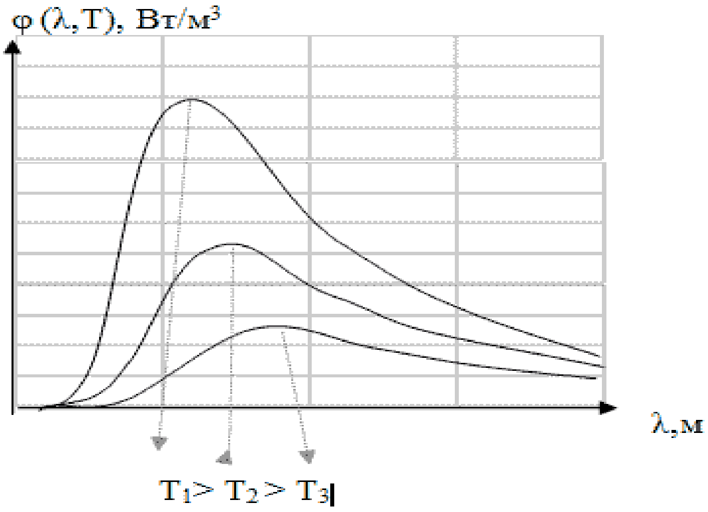


Fig. 1.2.2 – Thermal radiation

Infrared radiation is a type of electromagnetic radiation that falls within a certain range of wavelengths on the electromagnetic spectrum. It is situated between visible light and microwave radiation, with the exact boundaries of the range being somewhat undefined. There are several different standards for classifying infrared radiation based on wavelength. According to the International Commission on Illumination, infrared radiation is divided into three ranges:

1. IR-A (700-1400 nm)

2. IR-B (1400-3000 nm)

3. IR-C (3000 nm-1 mm).

The ISO 20473 standard divides infrared radiation into three ranges:

1. near infrared (780-3000 nm)

2. mid-infrared (3000-50,000 nm)

3. far infrared (50-1000 microns).

In astronomy, infrared radiation is typically classified into three ranges:

1. near infrared (700-5000 nm)

2. mid-infrared (5000-25-40 microns)

3. far infrared (25-40-200-350 microns).

About 52% of the total intensity of sunlight that reaches the Earth's surface on a sunny day is in the infrared range.

Another way to classify infrared radiation is based on the sensitivity of different types of detectors. According to this classification scheme, there are five ranges of infrared radiation:

Near-infrared radiation: This range extends from 700 to 1000 nm, and is detectable by both human eyes and silicon detectors.

Short-wave infrared radiation: This range extends from 1 to 3 microns, and is detectable by silicon detectors and less sensitive detectors based on lead salts. InGaAs detectors are capable of detecting wavelengths up to 1.8 microns in this range.

Mid-wave infrared radiation: This range extends from 3 to 5 microns, and is detectable by detectors based on indium antimonide (InSb), HgCdTe, and partially PbSe.

Long-wave infrared radiation: This range is defined as either 8 to 12 microns or 7 to 14 microns, and is detectable by HgCdTe-based detectors and microbolometers.

Very long-wave red radiation: This range extends from 12 to 30 microns, and is detectable by doped silicon-based detectors.

Additionally, the radiation coefficient of materials determines their physical properties in the absorption and emission of thermal energy (as shown in Table 1.2.1).

Table 1.2.1 – Emissivity coefficients of various materials

| Material | thermal emissivity |
|---|---|
| Aluminium, polished | 0.05 |
| Aluminium, strongly oxidized surface | 0.25 |
| Aluminium, rough surface | 0.07 |
| Asbestos paper | 0.94 |
| Asbestos panel | 0.9 |
| Asbestos fabric | 0.78 |
| Asbestos-cement slab | 0.96 |
| White tin, polished | 0.05 |
| Concrete | 0.54 |
| Bronze, porous, rough | 0.55 |
| Paper, white | 0.90 |
| Paper, black, glossy | 0.90 |
| Paper, black, matte | 0.94 |
| Water | 0.98 |
| Tungsten | 0.05 |

| | |
|---|---|
| Clay, fired | 0.91 |
| Iron, shiny, poisons the surface | 0.16 |
| Iron, hot rolling | 0.77 |
| Iron, forged, polished surface | 0.28 |
| Iron, oxidized surface | 0.74 |
| Iron, galvanized sheet, oxidized | 0.28 |
| Iron, galvanized sheet, polished | 0.23 |
| Gold, polished | 0.02 |
| Insulating tape, black | 0.95 |
| Quartz | 0.93 |
| Brick, glazed, rough | 0.85 |
| Brick, ordinary | 0.85 |
| Brick, refractory, rough | 0.94 |
| Paint, oil, ordinary | 0.94 |
| Paint, silver | 0.31 |
| Varnish, Bakelite | 0.93 |
| Varnish, white | 0.87 |
| Varnish, black, glossy | 0.87 |
| Varnish, black, matte | 0.97 |

| | |
|---|---|
| Lamp soot | 0.96 |
| Brass, polished | 0.03 |
| Brass, dull surface | 0.22 |
| Ice | 0.97 |
| Copper, oxidized | 0.65 |
| Copper oxidized to black | 0.88 |
| Copper, polished | 0.01 |
| Copper, commercial, polished | 0.07 |
| Frozen ground | 0.93 |
| Nickel, on cast iron | 0.05 |
| Nickel, pure, polished | 0.05 |
| Platinum, clean, polished | 0.08 |
| Rubber | 0.93 |
| Mercury, pure | 0.10 |
| Ruberoid | 0.92 |
| Lead, shiny surface | 0.08 |
| Lead, oxidized surface | 0.63 |
| Lead, Gray | 0.28 |
| Lead marmot, powder | 0.93 |
| Snow | 0.80 |
| Steel, sheet, katana | 0.56 |

| | |
|---|---|
| Steel, sheet, nickel-plated | 0.11 |
| Steel, galvanized | 0.28 |
| Steel, rust | 0.69 |
| Steel, freshly rolled | 0.24 |
| Steel, heavily oxidized | 0.88 |
| Steel, rough surface | 0.96 |
| Glass | 0.92 |
| Frosted glass | 0.96 |
| Carbon, refined | 0.80 |
| Charcoal, powdered | 0.96 |
| Porcelain, glazed | 0.92 |
| Chrome, polished | 0.10 |
| Zinc, sheet | 0.20 |
| Cast iron, polished | 0.21 |
| Cast iron, rough surface | 0.81 |
| Shellac, black, glossy | 0.82 |
| Shellac, black, matte | 0.91 |
| Enamel | 0.90 |
| Melamine | 0.93 |

## 1.3 Classification and characteristics of thermal imagers

Thermal imaging devices are used to detect objects by sensing the thermal radiation they emit. These devices work by converting infrared radiation into visible wavelengths, allowing them to create images based on the temperature of an object. The range of wavelengths that thermal imagers can detect is determined by the energy range of the objects being observed. Typically, thermal imagers operate in the 3.5-5.5 µm or 8-13.5 µm wavelength intervals.

Modern thermal imagers are highly sensitive and can detect temperature differences of even hundredths of a degree. They are used in a variety of industries, including medicine and military applications, and can produce images with television-level resolution.

The first thermal imaging device, known as a vaporograph, was developed in the late 1920s. It used a membrane to visualize the thermal image, but had low sensitivity and produced low-contrast images. In the 1940s, two main types of thermal imagers emerged: those that used optical-mechanical scanning to convert an infrared optical signal into an electrical signal, and those that used electronic scanning with infrared vidicons, pyricons, and matrix radiation receivers.

Most thermal imagers currently in use are based on the first principle, but matrix radiation receivers, which function through charge accumulation, are becoming increasingly popular due to their superior consumer properties.

Figure 1.2 shows a generalized functional diagram of a thermal imager with a focal IR matrix.

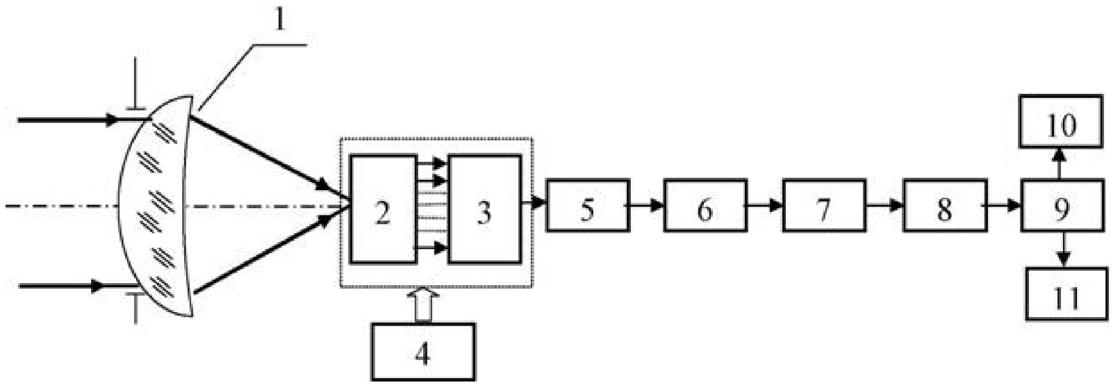


Figure 1.3.1 - Generalized functional scheme of a thermal imager with a focal matrix: 1 - optical system, 2 - focal matrix with preamps, 3 - multiplexer, 4 - cooling system, 5 - corrector of inhomogeneity of the characteristics of sensitive elements; 6 - analog-digital converter, 7 - digital non-uniformity corrector; 8 - corrector of non-working cells; 9 - image former, 10 - display, 11 - digital output.

Focal infrared matrices are used in thermal imaging devices to detect and convert infrared radiation into a usable electrical signal. These matrices come in a range of sizes, including 128x128, 256x256, and 512x512 elements, with each element measuring 30x30 μm2.

Focal matrices are self-contained photo-receiving devices that include a cooling system, preamplifiers, a multiplexer, a corrector for inhomogeneities in the characteristics of sensitive elements, an analog-to-digital converter, digital processing units, and a signal output generator. The signals produced by these devices can be transmitted to a video control device or to digital processing units in digital form.

Figure 1.3.2 shows a generalized functional diagram of a thermal imager with an optical-mechanical scanning system.

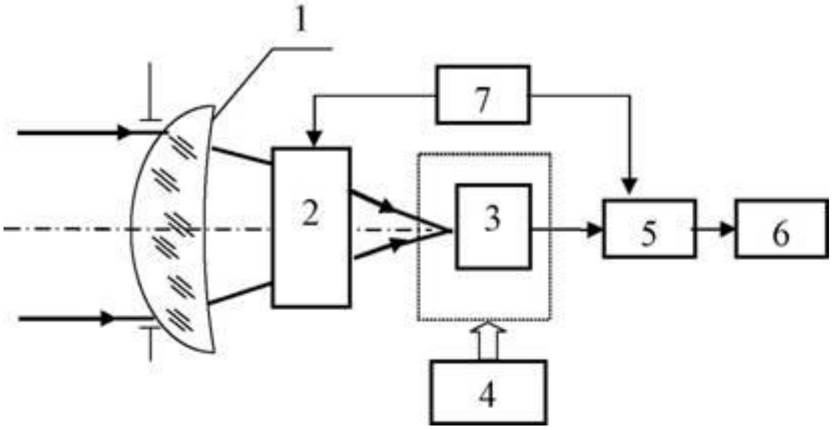


Figure 1.3.2 – Generalized functional diagram of a scanning thermal imager: 1 - optical system, 2 - optical-mechanical scanning unit, 3 - radiation receiver, 4 - cooling system, 5 - electronic path, 6 - video control device, 7 - synchronization system.

### 1.4 Characteristics of the used thermal imager

The FLIR i7 thermal imager, which complies with the RESNE standard, was used in the research. This device features a CCD matrix with a resolution of 140x140 pixels and an accuracy of 2%. It has a sensitivity for temperature measurement of 0.1ºC.

Some of the main characteristics of the FLIR i7 thermal imager include:

- Infrared resolution: 120x120 pixels
- Weight: 340 g
- Temperature sensitivity: <0.1°C at 25°C
- Hyperfocal capability
- A 2.8-inch color liquid crystal display (LCD)

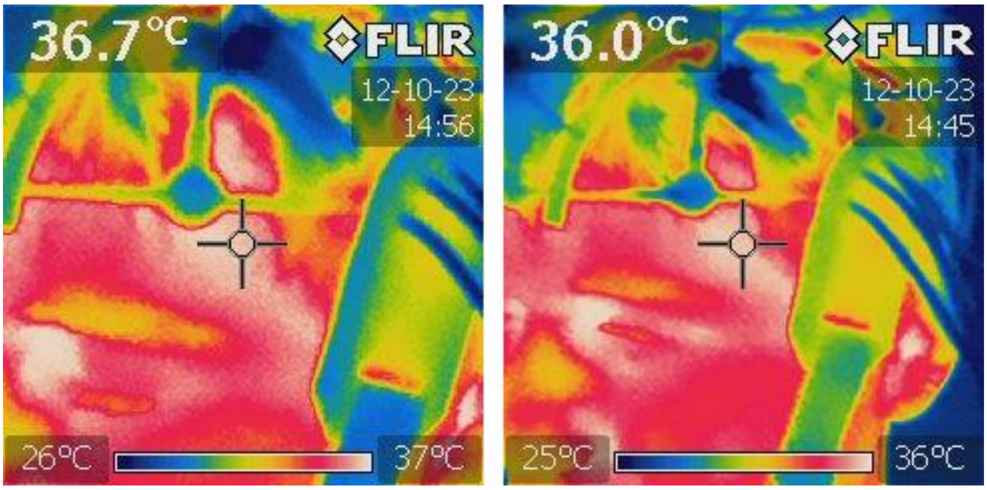


Figure 1.3.3 – Thermographs made with the FLIR i7 thermal imager

# 2. METHODS OF ANALYSIS

## 2.1. The theory of thermal image data determination

A thermal imager is a device used to monitor the temperature distribution of an object. It works by using a matrix of sensors known as a CCD (charge coupled device) to send a signal to a decoder, which is then processed by a central microprocessor and displayed on a liquid crystal display.

The FLIR QuickReport software, which is a part of the FLIR i7 thermal imager system, allows users to analyze the temperature of every thermal pixel in an image captured by a FLIR camera. This software is often used in the preventive maintenance of electrical and energy systems to detect malfunctions, but it can also be used in medical diagnostics, particularly in the diagnosis of heart and blood vessel conditions.

The development of specialized algorithms for processing and analyzing thermal images is necessary for this application. In the development of thermal image processing software, various mathematical methods are used to compare the temperature range and color gamut of the infrared image.

The temperature distribution image on the display is made up of tiny pixels, each of which is a specific color based on the selected color palette and represents the temperature of the object being studied.

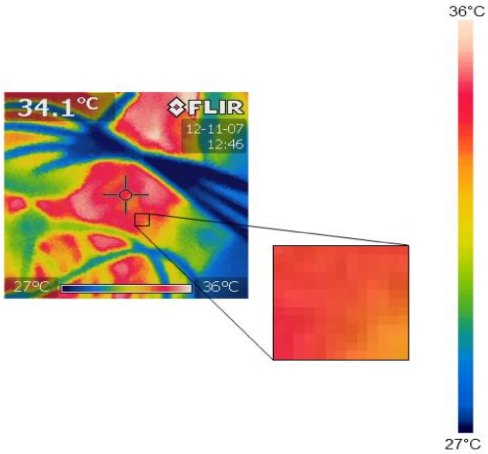


Figure 2.1.1 – Constituent parts of the image of the thermal imager

In thermal imaging, each pixel represents the temperature of a specific area, such as a blood vessel, based on the chosen color palette. The temperature of a particular point on the thermogram is determined by comparing the pixel color to the colors on the thermogram's color palette and using the minimum and maximum temperature data for the thermogram. The color determination in this program is done using the RGB color model, in which each color is represented by variations of the red, green, and blue channels. This allows for accurate temperature readings to be taken from thermal images of the human brain (Fig. 2.2.1).

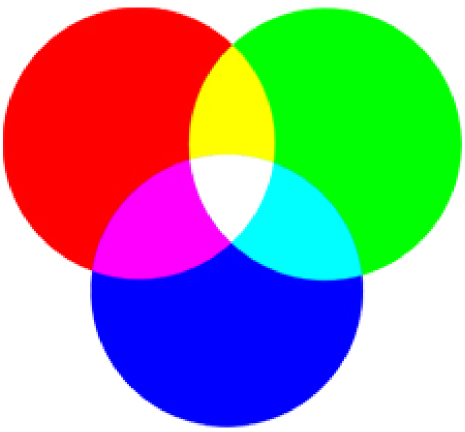

Figure 2.2.1 – The principle of mixing colors in the RGB model

## 2.2 Software implementation of thermal image data determination

To make it easier to analyze thermograms, the FLIR WebViewer program is used to convert the color thermogram of the brain's atria to black and white (Fig. 2.2.2). The resulting black and white image is then analyzed using a program written in Object Pascal in the Lazarus software development environment (version 1.0.6). The output of this program is saved in a file and further analyzed using the OpenOffice office package (version 3.4.1), specifically using the OpenOffice Calc tool for processing tables.

The software processing was performed using two thermal images of the blood vessels in the temporal region of the brain, taken with a FLIR i7 thermal imager at a temperature of 31.9 ºC.

The presentation of the thermographic images in the working window of the program developed for analyzing thermogram data is shown in Figure 2.2.3. The black and white thermogram of the brain is used for the analysis of thermal images of the brain's blood vessels because it increases the contrast of the image and clearly shows the blood vessels. This filtering of the thermogram image also improves the accuracy of matching the pixels of the image to the local temperature in the area.

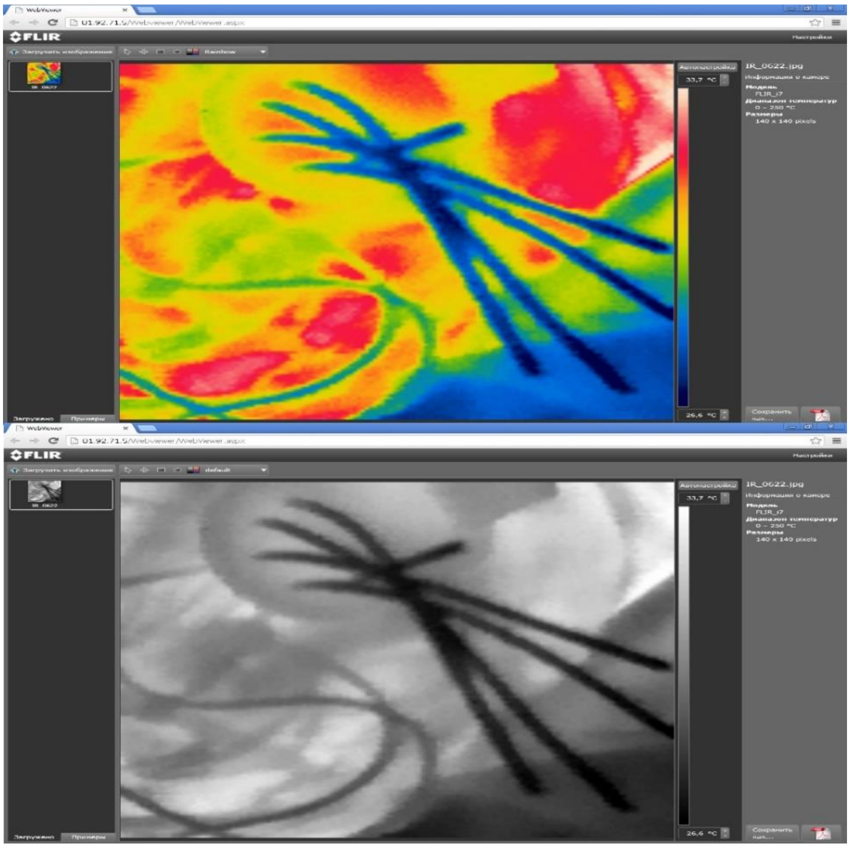


Figure 2.2.2 - FLIR WebViewer program window

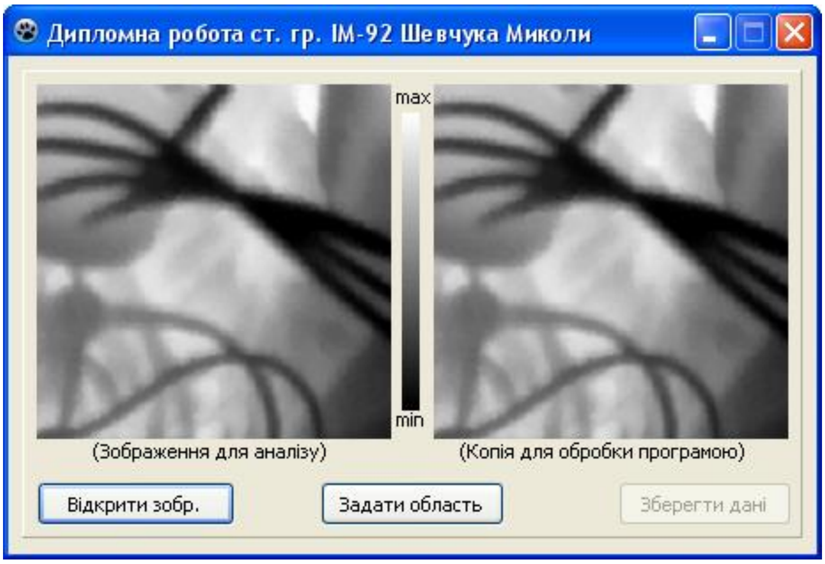


Figure 2.2.3 – Software implementation of thermal image analysis of human brain arteries

The black and white thermogram of the human brain's arteries, obtained using the FLIR WebViewer program developed in the Lazarus environment, is analyzed using the following algorithm:

1. The user defines the area of the image to be analyzed.
2. The program analyzes each pixel in the selected area and writes the value of one of the colors to an array (since it is a black and white image, R=G=B), converting values from 1 to 100.
3. If a color, according to the color palette, has a value of 0, it is assigned a value of 1.

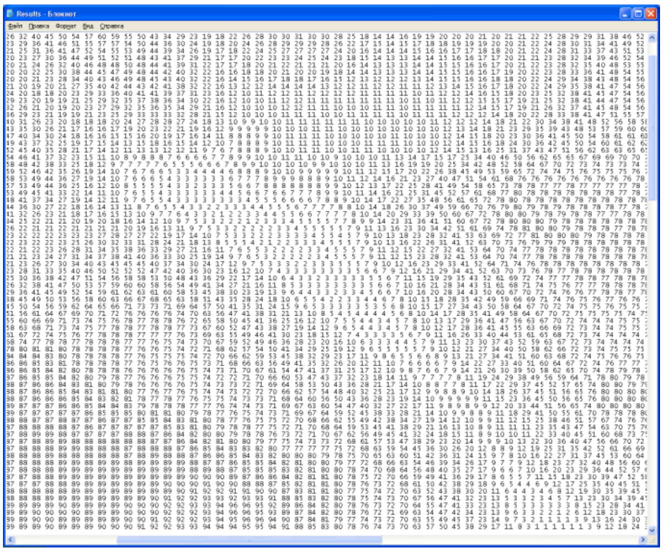

Figure 2.2.4 – Results of program analysis

## 2.3 Data processing in the OpenOffice office suite

The arrays of temperature data for selected parts of the image before and after a patient's operation were analyzed in OpenOffice Calc. The data arrays were compared by calculating the sample variance of the rows in the first and second images using the following formula:

$$D_{\text{г}} = \frac{\sum_{i=1}^{n}(x - \bar{x})^2}{n}$$

The results of the statistical analysis, shown in fig. 2.3.1, are the variance values in the columns of the data array for two images.

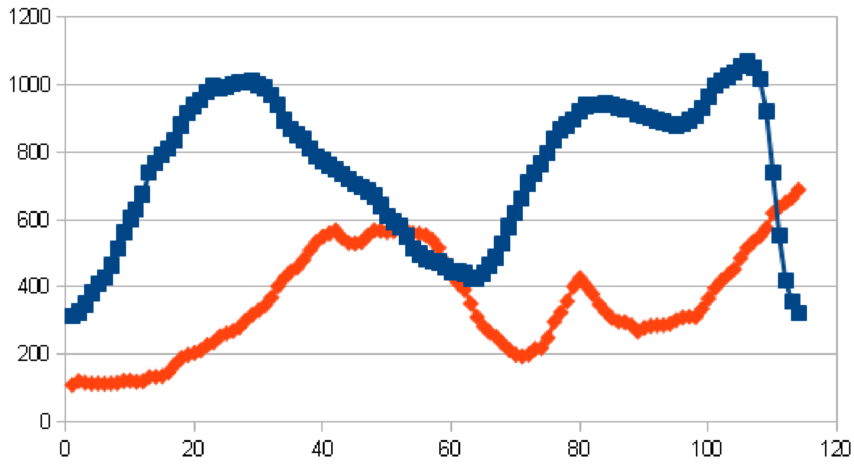


Figure 2.3.1 – Line variances of two images

The maximum value is 1066.77, the minimum is 109.61, and the average value is 554.10. The average of the absolute values of deviations of the data points from the average is 2.32%, which is above the 2% error of FLIR i7 thermal imaging images and therefore indicates the reliability of the chosen method.

A comparison of the variance dependencies for the two thermographic images of the blood vessels in the temporal region of the brain on both sides of the head reveals the symmetry of the temperature profile in local areas along the selected direction (as shown by the columns of the data array).

By examining the temperature distribution and the level of dispersion in certain areas of the thermogram, it is possible to assess the condition of the blood vessels of the brain, such as the presence of pathological expansion, tumors, blood clots, or arteriovenous shunts.

The data from the two images were also analyzed using line correlation to determine the repeatability of the results, using the following formula:

$$Correl(X,Y) = \frac{\sum (x-\bar{x})(y-\bar{y})}{\sqrt{\sum (x-\bar{x})^2 \sum (y-\bar{y})^2}}$$

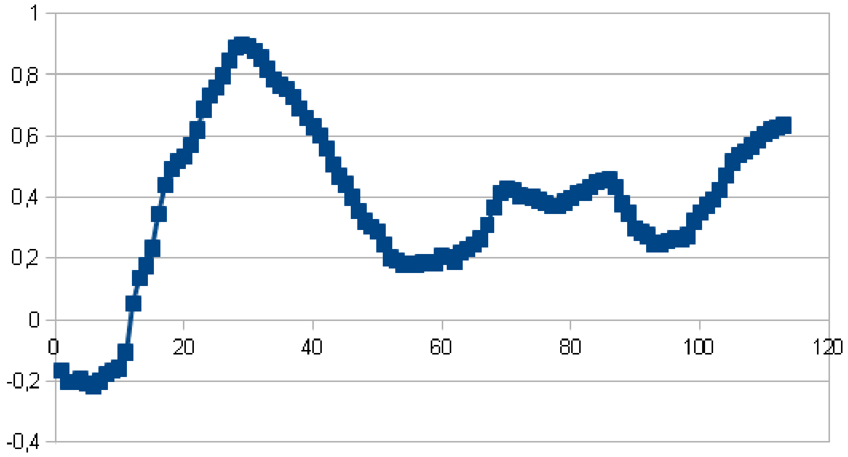


Figure 2.3.2 – Line correlation of two images

The maximum value is 0.90, the minimum is -0.22, and the average value is 0.38, which indicates the repeatability of the research results when obtaining thermographic images of the blood vessels in the temporal region of the brain on both sides of the head.

In further studies, it is planned to compare the thermal image data with electrocardiogram data in patients before and after artificial blood circulation.

Figures 2.4.1, 2.4.2, 2.4.3, and 2.4.4 show the results from clinical practice, including the patient's electrocardiograms before and after aortic valve replacement.

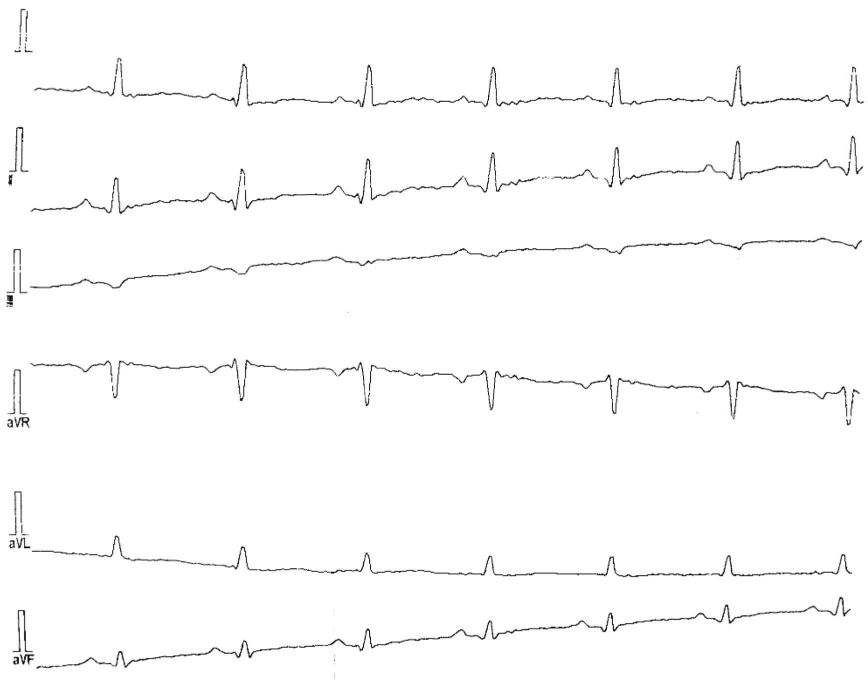


Figure 2.4.1 – Electrocardiogram of the patient before prosthetics aortic valve

Figure 2.4.2 – Electrocardiogram of the patient after prosthetics aortic valve

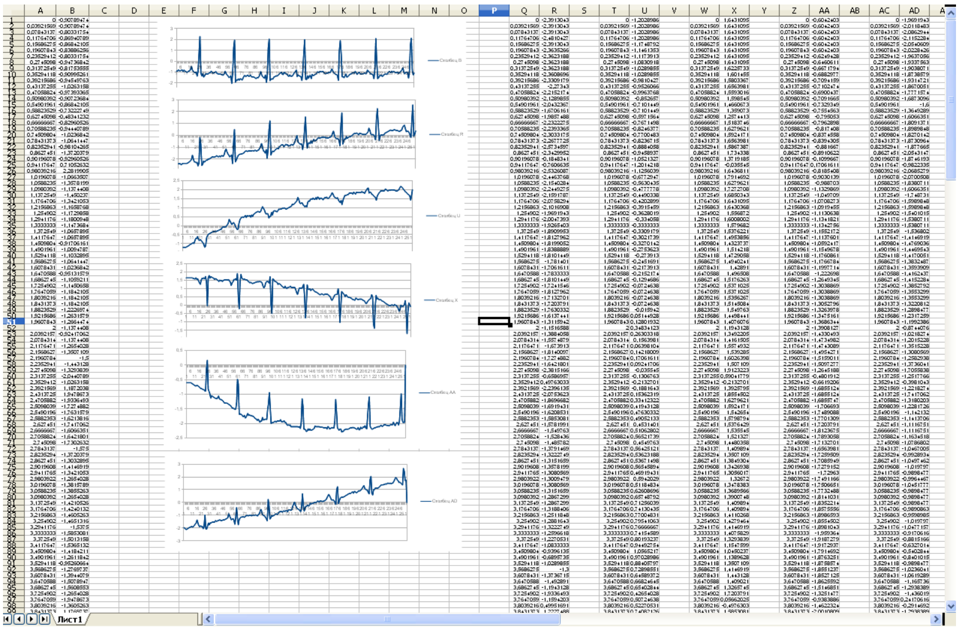

Figure 2.4.3 – Digitized electrocardiograms of the patient aortic valve prosthetics

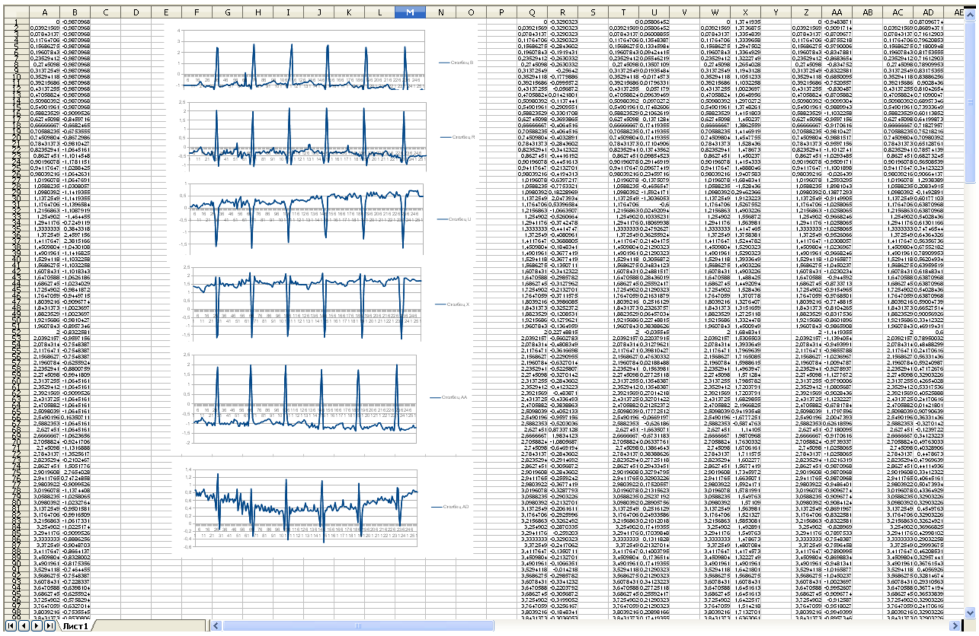

Figure 2.4.4 – Digitized electrocardiograms of the patient after aortic valve prosthetics

# 3. LABOR PROTECTION

## 3.1 Introduction

Thermographs are used to identify pathologies in human brain arteries by allowing for a qualitative assessment of the surface temperature of the human body and the detection of early-stage pathologies. Occupational health and safety authorities recognize that the use of thermography requires specialized training to minimize the risk of harm to workers and maximize their efficiency. The following recommendations have been made by national and international bodies to protect the health and safety of workers during thermographic imaging procedures:

• Training in basic workplace safety and ergonomic principles should be provided to all workers performing scanning procedures using thermal imaging equipment.

• Work environments should be designed to minimize exposure to hazardous physical agents and biological hazards.

• Workers should use appropriate personal protective equipment and handle radioisotopes under close supervision.

• Workplace noise should be controlled to avoid excessive levels of sound pressure level exposure in the workplace.

• Workers should wear disposable clothing and gowns when performing radioisotope procedures to ensure that they do not come into contact with radioactive isotopes during scanning operations.

This section discusses the regulations regarding the safety and protection of workers who use thermal imaging analysis equipment.

## 3.2 General characteristics of a room with a thermal imaging device diagnostic

The dimensions of the room are 5 meters wide, 4.2 meters long, and 3 meters high, with a total area of 21 square meters. The room has a capacity of 3 people and a volume of 63 cubic meters.

Table 3.1 - Objects in the room

| Element | Number in the scheme |
|---|---|
| Bed for medical examination | 1 |
| Chair | 2 |
| Table | 3 |
| Personal Computer | 4 |
| Wardrobe | 5 |
| Internal door | 6 |
| External door | 7 |
| Tap | 8 |
| Window | 9 |

The plan of the room is presented in fig. 3.1.

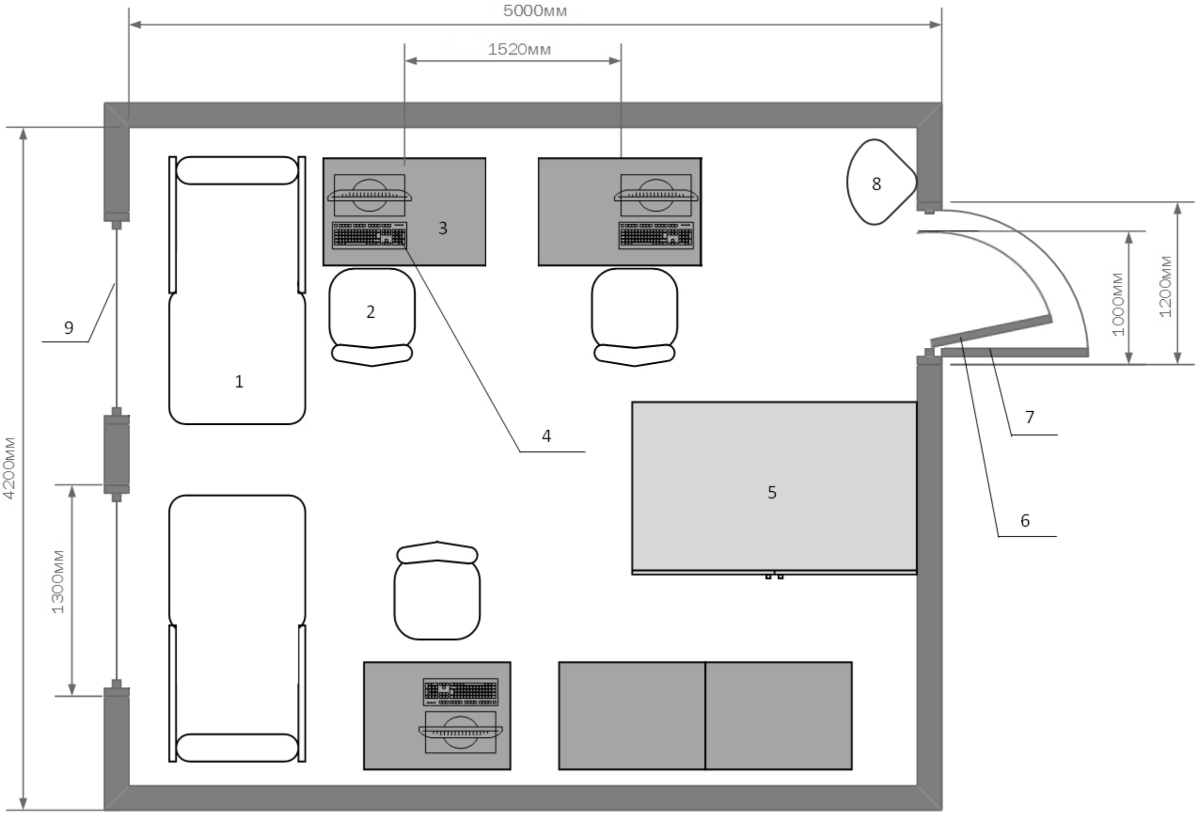


Fig. 3.1 - Plan of the room

The compliance of the available parameters with the norm is given in the table. 3.2

Table 3.2 - Compliance of room parameters with sanitary and hygienic standards

| Parameter | Following parameters | Norm |
|---|---|---|
| Area for 1 person, S | 7 m2 | not less than 6 m2 |
| Volume for 1 person, V | 21 m3 | not less than 20 m3 |
| The width of the external door, L1 | 1.2 m | not less than 1 m |
| The width of the internal door, L2 | 1 m | not less than 1 m |
| Distance between computers | 1.5 m | not less than 1.5 m |

The room's parameters comply with the established norms, which ensures the safe use of the thermal imaging device and the study of human body temperature.

### 3.3 Assessment of dangerous and harmful production factors

Table 3.3 – Dangerous and harmful production factors

| Factors | Causes of occurrence |
|---|---|
| Physical | • adverse microclimate conditions;<br>• insufficient lighting and increased light brightness;<br>• noise;<br>• radiation when working with computing equipment. |
| Chemical | - |
| The danger of impression el. current | • accidental contact with parts that conduct current and are under voltage;<br>• appearance of voltage as a result of erroneous switching on, short-circuiting or voltage induction by neighboring installations. |
| Fire hazard | • Short circuit, sparking in contacts, long overloads. |

#### 3.3.1 Microclimate

Table 3.3.1.1 - Actual values of temperature, humidity and speed of air movement in the office

| Period of the year | Air temperature | Relative humidity |
|---|---|---|
| Cold | 22 $^0$C | 50 % |
| Warm | 23 $^0$C | 45 % |

The thermography procedure and analysis of thermograms involve minimal physical effort and can be performed while sitting or standing. Therefore, these tasks fall under the category of "Light work - 1b," according to DSN standard 3.3.6.042-99. This standard state that:

Table 3.3.1.2 – Obtained microclimate parameters

| Period of the year | Air temperature | Relative humidity | Speed of movement |
|---|---|---|---|
| Cold | 22-23 $^{0}$C | 60-40 % | 0,1 m/s |
| Warm | 22-24 $^{0}$C | 60-40 % | 0,1 m/s |

The microclimate in this office meets the standards, with heating used during the cold season and an air conditioner used for air conditioning during the warmer months.

Table 3.3.1.3 – Characteristics of the air conditioner

| | |
|---|---|
| Type | Split system |
| Brand | Honda HD-07HR4F/V |
| Dimensions (height - width - depth) | 0.25m - 0.71m - 0.19m |
| Modes | Cooling/heating/drying |
| Power consumption | 0.73 kW |
| Power in cooling mode | 2.1 kW |

### 3.3.2 Lighting

Both natural and artificial lighting are used in the room. The natural lighting comes from two east-facing windows, measuring 1.3m x 1.8m, with double-glazed metal-plastic windows. The smallest objects that we work with are displayed on the screen of a Samsung SyncMaster 795DF monitor. The development environment program, Lazarus, has a light grey background. The smallest resolution object size is approximately 0.2 mm, allowing for high accuracy in visual work.

Table 3.3.2.1 – Characteristics of visual work

| Characteristics of visual work | Very high accuracy | |
|---|---|---|
| The smallest size of the resolution object, mm | From 0.15 to 0.3 mm | |
| Category and subcategory of visual work | II B | |
| The contrast of the discrimination object with the background | Average | |
| Characteristics of the background | Average | |
| Natural lighting | Lateral | 1.5 |

Table 3.3.2.2 – Artificial lighting

| Type of lighting | Combined |
|---|---|
| The number of lamps | 2 pieces |
| Series | LPO-12 (dimensions 1245×75×180) |
| Type of lamps | LPO 2x40 |
| The shape of the diffuser | Rectangular |
| Number of lamps | 2 |
| Height from the floor | 2.8 m |

Table 3.3.2.3 – Real and normative values of illumination

| Degree of visual work | Light | | |
|---|---|---|---|
| | Combined lighting | General lighting | general lighting (real value) |
| II в | 2000 lm | 550 lm | 3200 lm |

The lighting meets the established standards for optimal performance.

### 3.3.3 Noise

Table 3.3.3.1 – Sources of noise

| Source of noise | Equivalent noise level | Permissible noise level in this room, dBA |
|---|---|---|
| Computer (system unit) | 12 dB | 50 |
| External noise | 40 dB | |

The sound level in the room is within the established norm of 50 dBA, as specified in DSN 3.3.6.037-99 "Sanitary standards for industrial noise, ultrasound and infrasound."

Table 3.3.3.2 – Measures and means of protection against noise

| Kinds | Description |
|---|---|
| Technical | • In the source of occurrence;<br>• On the path of distribution (metal-plastic windows). |
| Personal protective equipment | • Anti-noise inserts;<br>• Headphone. |

### 3.3.4 Radiation

The office has a low level of electromagnetic radiation due to the use of an electron beam tube in the PC monitor, which emits a small amount of electromagnetic radiation. There are no infrared or ultraviolet radiations present.

### 3.3.5 Electrical safety

The main electrical appliances in this office include PCs, lighting sources, and air conditioners, which do not pose a significant risk of electric shock. The equipment is connected to an alternating current network with a voltage of 220 V and a frequency of 50 Hz. However, there is still a potential for electric shock due to insulation failure or lack of reliable grounding and non-compliance with safety rules. The thermal imager operates with a universal power source and is connected to the computer using an insulated wire to the USB bus, which prevents the risk of electric shock.

Table 3.3.5.1 – Voltage consumption parameters

| Source of voltage consumption | High-voltage |
|---|---|
| PC | 250 W |
| Lamplight | 60 W |
| Monitor | 80 W |
| Thermal imager adapter | 90 W |

Table 3.3.5.2 – Measures and means of protection against electric current

| Kinds | Description |
|---|---|
| Technical | • In the normal mode of operation of the equipment (isolation and inaccessibility of current-carrying parts, lamps - at a height of 2.8 m); • In emergency mode of operation (grounded sockets). |
| Organizational | All employees are familiar with safety regulations. |
| Means | • Electric tool with dielectric handles; • Protective mats, dielectric stands. |

### 3.3.6 Fire safety

Possible causes of fire in the office include:

- Malfunctioning of electrical equipment and overloading of the electrical network
- Non-compliance with the rules for operating equipment and electrical devices
- Violation of fire safety protocols, such as using household heating devices or smoking.

Table 3.3.6.1 – Characteristics of the fire hazard of the premises

| Fire classification | A; E |
|---|---|
| Category | B |
| Fire hazard classification | P-Iia |
| Flammable substances | Papers, tables, chairs, cabinets, plastic bodies. |
| Thermal fire alarm sensors | KI-1. Dimensions 100x45mm |
| Fire extinguishers | OU-3, 2 pieces. |

Also, the office provides free access to circuit breakers and switches to prevent fire.

### 3.4. Conclusion

This section discusses the rules and measures for occupational health and safety, which aim to eliminate potentially harmful and dangerous production factors. The microclimate parameters in this office meet the established standards, and the necessary means and measures are used to maintain these levels. The noise level in the office complies with regulatory limits. Safety measures against electric shock are also in place. Measures to protect working personnel from fire are also addressed and all parameters meet the necessary standards.

# CONCLUSION

The use of digital filtering of thermogram images with the FLIR WebViewer software increases the accuracy of determining the local temperature in an area, while the conversion of thermograms to black and white with the developed program enhances image contrast and highlights brain arteries. The resulting temperature profile dispersion graphs for human brain arteries demonstrate that the proposed analysis method can be used to assess the state of brain vessels and diagnose pathologies.

Comparison of variance dependencies for two thermographic images of brain vessels in the temporal region allows for the detection of pathological vessel expansion, tumours, blood clots, and arteriovenous shunts. The findings of this study can be applied in the analysis of thermal images of human brain arteries, considering the error of the thermal imager and the principles of the program.

Further research is needed to develop a standardized methodology to determine the temperature of different areas of the brain based on the measured values of water temperature in the brain using radio thermography.

## REFERENCES

1. Handbook on the Basics of Infrared Technology / ed.: L. Z. Kriksunov.: "Soviet Radio" Publishing House, 1978 - 400 p.
2. Thermal imagers: reference book / ed. L. Z. Kriksunov, G. A. Padalko.: "Technika" Publishing House, 1987 - 166 p.
3. FLIR. User's manual, 2011 - 178 p.
4. Infrared radiation of heated bodies / ed.: Bramson M.A.: "Nauka" Publishing House, 1964 - 226 p.
5. Infrared radiation / ed.: Hecford G.L.: "Energiya" Publishing House, 1964 - 335 p.

**APPENDIX A**

Program text

```
unit Unit1;

{$mode objfpc}{$H+}

interface

uses

  Classes, SysUtils, FileUtil, TAGraph, TARadialSeries, TASeries, Forms,

  Controls, Graphics, Dialogs, StdCtrls, ExtCtrls, shellapi, LCLIntf, Math;

type

  { TForm1 }

  TForm1 = class(TForm)

    Button2: TButton;

    Button3: TButton;

    Button4: TButton;

    Image2: TImage;

    Image3: TImage;

    Image4: TImage;

    Image5: TImage;

    Label1: TLabel;

    Label2: TLabel;

    Label3: TLabel;

    Label4: TLabel;
```

```
    OpenDialog1: TOpenDialog;
    Panel2: TPanel;
    procedure Button1Click(Sender: TObject);
    procedure Button1MouseDown(Sender: TObject; Button: TMouseButton;
      Shift: TShiftState; X, Y: integer);
    procedure Button2Click(Sender: TObject);
    procedure Button3Click(Sender: TObject);
    procedure Button4Click(Sender: TObject);
    procedure Button4MouseDown(Sender: TObject; Button: TMouseButton;
      Shift: TShiftState; X, Y: integer);
    procedure FormCreate(Sender: TObject);
    procedure Image4Click(Sender: TObject);
  private
    function zcolor(tr, tg, tb: integer): integer;
    function plt(): integer;
    { private declarations }
  public
    { public declarations }
  end;
var
```

```
  Form1: TForm1;
  d, d2, dnorm, d2norm: array [1..300, 1..300] of double;
  s: string;
  s2: array [1..200] of string;
  sl: TStringList;
  graph: boolean;
  tx, ty, tx1, ty1, tx2, ty2, k, kd, kd2, im, a, a2, nij: integer;
  List: TStringList;
  f: string;
implementation
{$R *.lfm}
{ TForm1 }
procedure TForm1.Button1MouseDown(Sender: TObject; Button: TMouseButton;
  Shift: TShiftState; X, Y: integer);
begin
  Label1.Caption := 'Обробка даних...';
end;
procedure TForm1.Button1Click(Sender: TObject);
begin
end;
procedure TForm1.Button2Click(Sender: TObject);
```

```
var
  filename: string;
begin
  if OpenDialog1.Execute then
  begin
    filename := OpenDialog1.Filename;
    image2.Picture.LoadFromFile(filename);
    image4.Picture.LoadFromFile(filename);
    button3.Enabled := False;
    button4.Enabled := True;
    label1.Caption := 'Файл ' + opendialog1.FileName;
    k := 1;
    button3.Enabled := False;
  end;
end;
procedure TForm1.Button3Click(Sender: TObject);
var
  i, j, a, tr, tg, tb: integer;
begin
  List.SaveToFile('./Results.txt');
  List.Free;
  showmessage('Дані успішно збережені!');
```

```
e nd;
procedure TForm1.Button4Click(Sender: TObject);
begin
  graph := True;
  image4.Picture.LoadFromFile(opendialog1.FileName);
  image5.Canvas.Clear;
  k := 1;
end;
procedure TForm1.Button4MouseDown(Sender: TObject; Button: TMouseButton;
  Shift: TShiftState; X, Y: integer);
begin
  Label1.Caption := '';
end;
procedure TForm1.FormCreate(Sender: TObject);
begin
  sl := TStringList.Create;
  graph := False;
  im := 1;
end;
procedure TForm1.Image4Click(Sender: TObject);
var
```

```
  f: Tpoint;
  i, nx1, ny1, nx2, ny2, k1, k2, c, c2, cx, cy, a, i1, j1, i2, j2: integer;
  s: string;
begin
  if (graph = True) then
  begin
    if (k < 3) then
    begin
      f := Form1.ScreenToClient(Mouse.CursorPos);
      tx := f.x - image4.Left - panel2.Left + 1;
      ty := f.y - image4.Top - panel2.Top + 1;
      image4.Canvas.RoundRect(tx - 2, ty - 2, tx + 2, ty + 2, 10, 10);
      if k = 1 then
      begin
        tx1 := tx;
        ty1 := ty;
        label1.Caption := 'Точка 1: (' + IntToStr(tx1) + ', ' + IntToStr(ty1) +
')';
        //im:=2;
      end;
      if k = 2 then
      begin
```

```
if (tx1 > tx) and (ty1 > ty) then
begin
  if im = 2 then
    a := a2
  else
    a := min(tx1 - tx, ty1 - ty);
  tx2 := tx1 - a;
  ty2 := ty1 - a;
end;
if (tx1 < tx) and (ty1 < ty) then
begin
  if im = 2 then
    a := a2
  else
    a := min(tx - tx1, ty - ty1);
  tx2 := tx1 + a;
  ty2 := ty1 + a;
end;
if (tx1 < tx) and (ty1 > ty) then
begin
  if im = 2 then
    a := a2
```

```
  else
    a := min(tx - tx1, ty1 - ty);
  tx2 := tx1 + a;
  ty2 := ty1 - a;
end;
if (tx1 > tx) and (ty1 < ty) then
begin
  if im = 2 then
    a := a2
  else
    a := min(tx1 - tx, ty - ty1);
  tx2 := tx1 - a;
  ty2 := ty1 + a;
end;
if (tx1 = tx) or (ty1 = ty) then
begin
  tx2 := tx1;
  ty2 := ty1;
end;
if im < 2 then
  a2 := a;
```

```
      label1.Caption := label1.Caption + ' Точка 2: (' + IntToStr(tx2) + ', ' + IntToStr(ty2) + ')';
    end;
  end;
  k := k + 1;
  if k = 3 then
  begin
    image4.Canvas.Pen.Style := psDash;
    image4.Canvas.Line(tx1, ty1, tx2, ty2);
    image4.Canvas.Line(tx2, ty2, tx1, ty2);
    image4.Canvas.Line(tx1, ty2, tx1, ty1);
    image4.Canvas.Line(tx1, ty1, tx2, ty1);
    image4.Canvas.Line(tx2, ty1, tx2, ty2);
    image5.Canvas.Brush.Color := clWhite;
    image5.canvas.Polygon([Point(-10, -10), Point(210, -10), Point(210, 210), Point(-10, 210)]);
    image5.Canvas.Rectangle(tx1, ty1, tx2, ty2);
    image5.Canvas.Brush.Color := clBlack;
    image5.canvas.Polygon([Point(tx2, ty2), Point(tx1, ty2), Point(tx1, ty1), Point(tx2, ty1)]);
    graph := False;
    plt();
```

```
 if im = 3 then
begin
  List := TStringList.Create;
  List.Add('Графік_1:');
  for i1 := 1 to a do
  begin
      for j1 := 1 to a do
    begin
      s := s + ' ' + IntToStr(trunc(d[i1, j1]));
    end;
    List.Add(s);
    s := '';
  end;
  List.Add(' ');
  List.Add('Графік_2:');
    for i1 := 1 to a do
  begin
    for j1 := 1 to a do
    begin
      s := s + ' ' + IntToStr(trunc(d2[i1, j1]));
    end;
    List.Add(s);
```

```
        s := '';
        button3.Enabled := True;
      end;
    end;
  end;
 end;
end;
function TForm1.zcolor(tr, tg, tb: integer): integer;
begin
 if trunc(tr/2.55)=0 then zcolor:=1 else zcolor:=trunc(tr/2.55);
end;
function TForm1.plt: integer;
var
 i, j, tr, tg, tb, a, b, nr, ng, minx, miny, maxx, maxy: integer;
begin
 if (tx2 <> tx1) and (ty2 <> ty1) then
 begin
  kd := 1;
  kd2 := 1;
  if tx1 < tx2 then
  begin
   a := tx2 - tx1;
```

```
  minx := tx1;
  maxx := tx2;
end;
if tx1 > tx2 then
begin
  a := tx1 - tx2;
  minx := tx2;
  maxx := tx1;
end;
if tx1 = tx2 then
begin
  a := 1;
  minx := tx1;
  maxx := tx2;
end;
if ty1 < ty2 then
begin
  b := ty2 - ty1;
  miny := ty1;
  maxy := tx2;
end;
if ty1 > ty2 then
```

```
begin
  b := ty1 - ty2;
  miny := ty2;
  maxy := tx1;
end;
if ty1 = ty2 then
begin
  b := 1;
  miny := ty1;
  maxy := tx2;
end;
nij := abs(a);
for i := 1 to abs(a) do
  for j := 1 to abs(b) do
  begin
    if image5.Canvas.Pixels[minx + i - 1, miny + j - 1] = clBlack then
    begin
      tr := getrvalue(form1.image2.Canvas.Pixels[minx + i - 1, miny + j -
1]);
      tg := getgvalue(form1.image2.Canvas.Pixels[minx + i - 1, miny + j -
1]);
```

```
          tb := getbvalue(form1.image2.Canvas.Pixels[minx + i - 1, miny + j -
1]);
          if im = 1 then
          begin
            d[i, j] := zcolor(tr, tg, tb);
            kd := kd + 1;
          end;
          if im = 2 then
          begin
            d2[i, j] := zcolor(tr, tg, tb);
            kd2 := kd2 + 1;
          end;
        end;
      end;
    if im < 3 then
    begin
    end;
    Label1.Caption := '';
    im := im + 1;
  end;
end;
```

**APPENDIX B**

A fragment of the calculation of variances of the program data

Sample variance (by series)

Chart 1:

314,3171091445

325,4712777519

348,1559540444

382,0807328055

407,9978264245

427,8842571029

463,4603322465

514,8772706102

561,8075609377

602,5334575377

628,7498835585

673,9146871604

740,3003415619

767,7696009936

790,7223257258

810,9117373079

835,7723955907

880,31827356

914,5596180717

937,5321378668

953,7857475547

978,3400093153

994,7897065673

990,3372147182

992,9173265021

1001,6659680174

1007,8094240025

1006,8223102003

1009,6138022046

998,9091755939

989,2480204937

967,4140661388

938,6682968483

893,9202763546

868,2369973607

851,7237230244

835,9184132899

811,446359261

785,8981524608

774,9508616674

760,7046266108

749,271308803

735,597267505

720,8695078404

705,5674584692

695,9180251514

684,1751280857

670,2612172023

640,9272628474

609,4081664338

593,946359261

578,3916317342

549,1145008539

514,8629871138

497,6364694923

482,2882316411

477,0979661543

472,8741655023

460,0537183667

444,8967551622

444,6176059618

439,8733115976

425,4892873777

426,0363297625

440,364229157

463,4202763546

487,8600372613

529,8462971588

578,8369042074

618,8067070331

663,5951715572

708,6312684366

737,0364850179

765,5843036796

795,9084769446

836,1857630803

865,2376960099

880,144775656

898,0497593541

920,569554417

936,5149045179

939,835739792

940,0158360503

944,021813383

939,1145008539

933,5746778451

927,6916627853

924,2919577705

913,7898618227

906,6064275734

902,8147803136

893,9465921441

889,0805775501

881,8003415619

880,1013041453

882,5766185375

894,0739791958

907,4386741189

929,9379754696

964,5127309424

995,9028101227

1010,4691818041

1023,2759664648

1036,2651762149

1055,8904673187

1066,7744915386

1049,820835274

1015,4936345288

919,3507219376

737,6839000155

552,6852973141

418,8713709051

355,1946126378

323,9568390002

Chart 2:

109,6057289241

120,8188169539

115,9668529731

113,6501319671

113,9264089427

112,866014594

113,9696475703

115,200201832

121,0861667443

121,747942866

118,8816177612

120,0553485484

133,7876106195

133,9652227915

135,3895357864

147,2433628319

170,5183201366

189,662474771

198,5763080267

204,4335506909

212,1441546344

227,4156186928

236,1757491073

253,871138022

262,2565595404

269,3185064431

280,5039590126

300,8048439683

317,3783573979

331,1278528179

345,4641360037

368,9126688402

402,4375097035

426,9272628474

445,9829219065

458,0220462661

481,1299487657

509,8580965689

534,3490141282

549,521813383

558,9715882627

567,6895668374

544,6648812296

530,7123117528

528,9952647104

533,3122185996

552,6176059618

567,506675982

566,6356932153

563,2206955442

565,1942244993

578,5111007608

567,3261915852

559,2886974072

557,9038192827

554,0693215339

539,9361124049

515,9696475703

475,0828287533

435,7072659525

411,8140816643

392,5483620556

350,7167365316

310,6971743518

282,8445893495

264,1682968483

251,6233504114

231,5914454277

213,7863685763

199,4023443565

194,5865548828

199,5532526005

216,0022512032

219,6795528645

249,2007452259

296,9181804068

324,6108523521

357,9435646639

401,597034622

426,3770377271

402,657351343

378,6005278683

348,2651762149

326,2567924235

307,1191585158

297,6569632045

295,6594472908

286,8713709051

267,9792734048

278,8772706102

284,5984319205

286,4121254464

286,9750815091

290,7020648968

301,97741034

309,2966930601

311,6156652694

310,7356000621

335,7563266574

366,0050458003

396,4692594318

418,4121254464

435,4063809967

452,7914920043

485,7917248874

515,5843036796

534,9507840397

550,4419344822

574,5164570719

618,8275888837

635,9333178078

650,2165036485

664,4214407701

688,3704393728

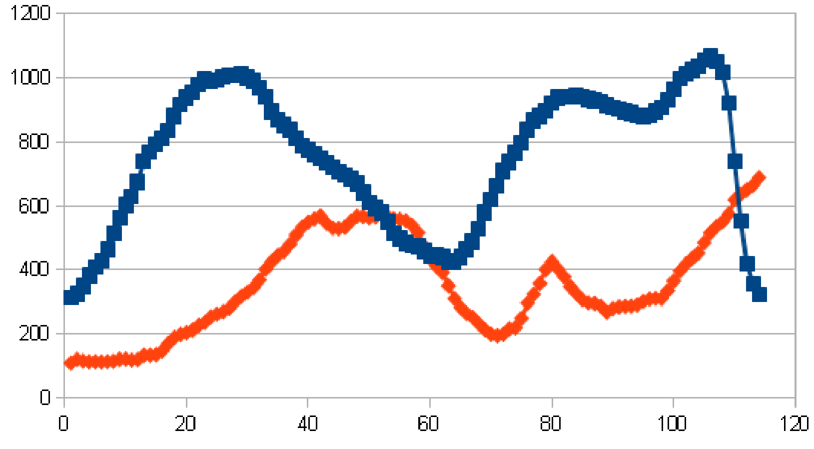


Figure B.1 – Dispersions along the lines of two images

**APPENDIX C**

A fragment of the program's data correlation calculation

-0,1295658269

-0,1662755962

-0,2020398982

-0,2018282444

-0,1952536511

-0,2063856974

-0,2194019282

-0,1991842545

-0,17647928

-0,1644015707

-0,1581551671

-0,1064427126

0,0533148223

0,1370453612

0,1757453388

0,2346043597

0,3456234575

0,4391719636

0,4929017115

0,5184451004

0,5322694314

0,5701220928

0,6205238719

0,6881238507

0,7309930356

0,7591706949

0,7968479466

0,8468154868

0,887080963

0,8976526489

0,8927108535

0,8795011398

0,8554404578

0,8179162593

0,7856467376

0,7654604945

0,7528945976

0,7264170806

0,68930312

0,6587881093

0,6300542689

0,6017158696

0,5609622442

0,5077424265

0,4691705619

0,442722365

0,4007606684

0,3556049084

0,3216855903

0,3027742768

0,2876632421

0,246445518

0,201207846

0,1957085851

0,1800691055

0,1803718684

0,1823480201

0,1864614089

0,1875333991

0,1876127428

0,2073832719

0,2055574469

0,1902772187

0,2214352577

0,2298813508

0,2465621499

0,2658255239

0,3105836266

0,3668913012

0,4137768671

0,4280201178

0,4239594278

0,4048256161

0,4041884231

0,4009937629

0,3901393464

0,3820158537

0,3722247879

0,3715162506

0,3851314428

0,3971442111

0,4140705678

0,416336304

0,4354772643

0,4510627176

0,4556604916

0,4568582849

0,433076867

0,3792159555

0,3486549574

0,3001875291

0,2854667825

0,2744751763

0,2487820185

0,2460834663

0,2569914186

0,2643705985

0,263524549

0,2752296318

0,3228171534

0,3512940146

0,3749557739

0,3940585939

0,4251309468

0,4705263022

0,5165472467

0,5399368055

0,5492202909

0,5668652535

0,5892229128

0,6061587068

0,620521151

0,6280236818

0,6353635671

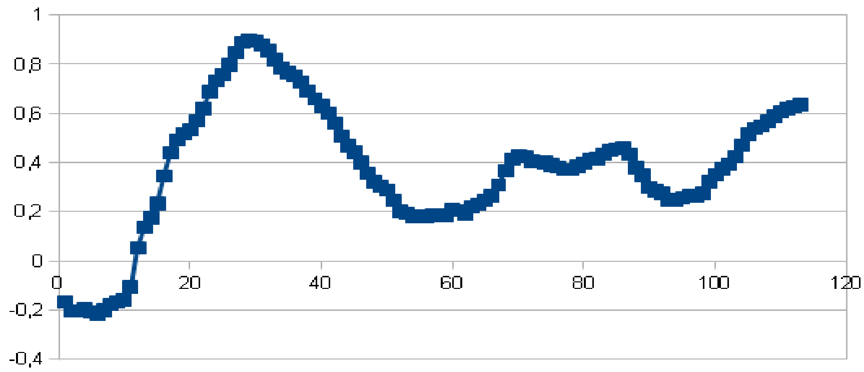


Figure B.1 – Row correlation of two images